A VERSATILE MARX GENERATOR FOR USE IN DIRECTED ENERGY AND EFFECTS TESTING APPLICATIONS

T. A. Holt[Ξ], J. R. Mayes, M. B. Lara, C. Nunnally, J. M. Byman, C. W. Hatfield
Applied Physical Electronics L C , PO Box 341149
Austin, TX, USA

Abstract

Applied Physical Electronics, L. C., (APELC) offers many Marx generators with stored energies ranging from 5 mJ to 1.8 kJ. The line of Marx generators offered by APELC can be used in a variety of applications including flash x-ray, high-power RF, high-power microwave, test and evaluation, triggering, and material studies. The MG15-3C-940PF (MG15), in particular, has seen wide use and integration into many systems over the past several years. The MG15 is a 33-J, 50-Ohm source and is capable of limited duty at 150 Hz at a maximum output voltage of 300 kV on to a matched load. The range of capabilities and custom configurations achieved by the MG15 as well as a sampling of the applications featuring the use of the MG15 will be presented. Recent additions to the capabilities of the MG15 include sub-ns rise time, jitter of less than 2 ns, and an energy density approaching 3.2 mJ/cm^3 (90 J/ft^3).

I. BACKGROUND

Applied Physical Electronics, L. C., (APELC) is a small company specializing in compact pulsed power, specifically Marx generators and custom high voltage solutions. An abridged listing of the Marx generators offered by APELC as COTS items is provided in Table 1.

The MG10-1C-1NF is the smallest Marx generator offered by APELC. The MG10-1C-1NF is fabricated from off-the-shelf components and a custom-made printed circuit board. APELC envisions its use as a trigger for larger pulsed power systems or as a direct RF source for small wideband antennas. This Marx generator is reported on further in [1].

The MG10-1C-940PF is a small Marx generator designed for integration into stand-alone, battery-powered systems. APELC uses this Marx generator for pulse-charging a capacitive load in one of its man-portable systems. The generator is capable of 10-Hz PRF and an erected voltage of 330 kV into an open circuit.

The MG30-3C-100NF, MG20-1C-100NF, and the MG20-22C-2000PF are all low-impedance Marx generators well suited for driving high-power microwave loads. Recently, the MG20-1C-100NF was used to support an HPM source development effort and demonstrated the capability to operate at a 10-Hz PRF at full charge voltage [2].

The MG16-3C-2700PF and the MG40-3C-2700PF both share the same stage topology with the main difference between the two Marx generators being the total number of stages comprising each one. The two aforementioned generators serve as a perfect example of the methods that can be employed to tailor an existing Marx generator design to a new application that might require more load voltage or a higher source impedance. The addition of stages to a Marx design (24 stages were added to the MG16-3C-2700PF to arrive at the MG40-3C-2700PF) increases the erected series inductance of the Marx while simultaneously reducing the erected capacitance thereby increasing the impedance of the Marx generator. This relationship is described in greater detail in [3].

The MG15-3C-940PF (MG15) is the subject of this paper and will be discussed in greater detail in subsequent sections. The 50-Ohm impedance of the generator makes it an ideal source for driving a coaxial cable which has

Table 1. Abridged summary of Marx generators offered by APELC.

Model Number*	Maximum Charge Voltage	Maximum Energy per Pulse	Peak Erected Voltage	Estimated Marx Impedance	Rise Time*	Pulse Width	Length	Housing Diameter/ (Width)	Maximum PRF**
	[kV]	*[J]*	*[kV]*	*[Ω]*	*[ns]*	*[ns]*	*[in]*	*[in]*	*[Hz]*
MG10-1C-1NF [1]	1	0.005	10	N/A	0.4	25	8	(2)	250
MG10-1C-940PF	33	5.1	330	N/A	N/A	N/A	16.7	3.1	10
MG15-3C-940PF	40	33	600	52	0.5 – 5	22	31 – 36	5	200
MG16-3C-2700PF	40	104	640	33	6 – 7	35	39	8	4
MG40-3C-2700PF	40	266	1,600	70	1 – 7	35	72	8	4
MG30-3C-100NF	20	1800	600	33	90	175	29	20	N/A
MG20-1C-100NF	20	400	400	25	~100	200	41	10	10
MG20-22C-2000PF	50	700	800	18	~20	80	60	19	SS
MG20x8-3C-2200PF-PFN	30	430	600	50-60	20	200	67.5	22	SS

* Rise times quoted using 10% - 90% standard.
** Verified values are often limited by the capability of the high voltage power supply used.

[Ξ]email: tholt@apelc.com

978-1-4577-0631-8/12/$26.00 ©2011 IEEE

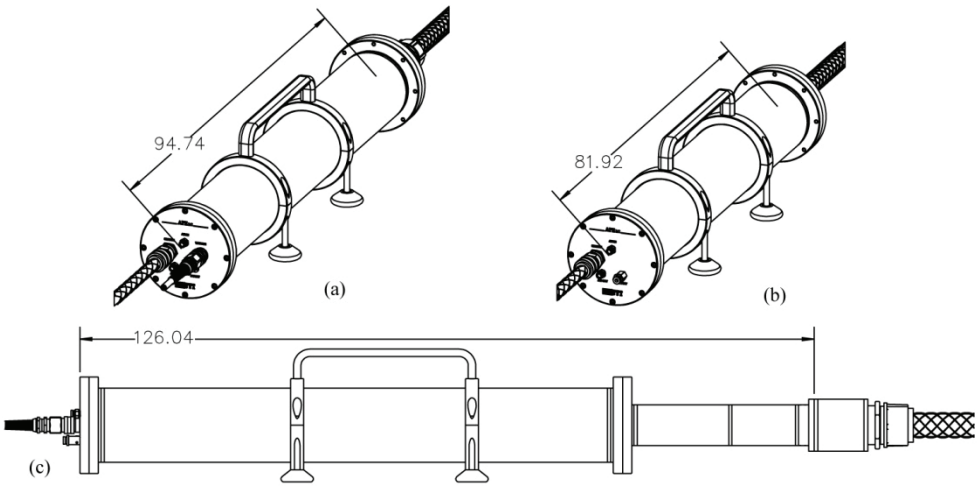

Figure 1 – All of the configurations of the MG15. (a) Standard configuration with a quick disconnect output cable assembly. (b) Miniaturized configuration with a pressurized output cable assembly. (c) MG15 as equipped with a peaking switch for sub-ns rise time. All drawings are on the same relative scale and all units are provided in cm.

led to wide adoption and integration into various systems performing many different functions. The wide use of the MG15, in turn, led to further development and refinement of the design, improving its reliability and extending the lifetime of the unit between maintenance periods. Several different configurations of the MG15 are depicted in Figure 1.

The majority of the Marx generators offered by APELC are designed to produce an output pulse opposite in polarity to the charge voltage polarity. The output MG15 waveforms presented in this manuscript have been inverted to facilitate their interpretation by the reader.

II. THE MG15-3C-940PF

MG15 specifications are listed in Table 1. A range of rise times and lengths are listed and are indicative of the different configurations available when ordering the MG15. Three different MG15 configurations are available and they are: the base configuration; the miniaturized configuration; and the base MG15 equipped with a modular peaking circuit designed to reduce the output pulse rise time.

A. Base Configuration

The base configuration of the MG15 has a flange OD of 16.5 cm, a housing OD of 12.7 cm, and a length of 95 cm. The base configuration also features a proprietary quick-disconnect output cable connection which facilitates servicing and manipulation of the MG15 as well as routing cables during installation.

The MG15 has proven its utility and reliability on numerous occasions in the past two years. The MG15 is the basis pulser used to pulse charge all of the high-power dipole transmitters APELC offers for E3 testing [4]. The MG15 has been delivered on numerous occasions as part of the E3 system and has demonstrated reliability, reproducibility, and a construction that facilitates standard maintenance.

Reproducibility of the MG15 is demonstrated in Figure 2 and Figure 3, where the electrical performance of the MG15 is quantified using the charge and output waveforms acquired during burst-mode operation at a pulse repetition frequency (PRF) of 200-Hz. A total of 18 charge cycles are captured in Figure 2. The reproducibility of the charge cycles indicates that sufficient dwell time is provided between shots for the spark gaps to recover prior to the application of the subsequent charge cycle.

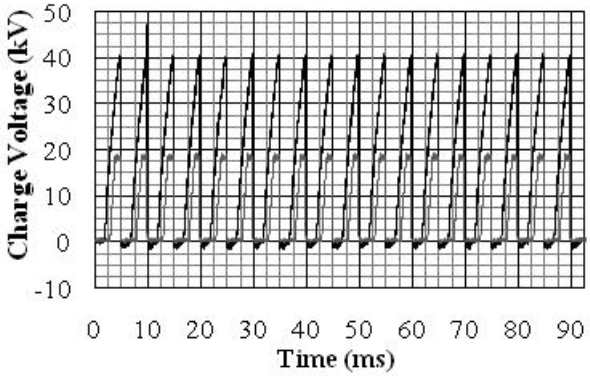

Figure 2. HVPS and trigger generator waveforms during burst mode operation at 200-Hz PRF.

A superposition of the 18 output waveforms corresponding to the charge cycles shown in Figure 2 is illustrated in Figure 3. While capable of 200-Hz operation, it is suggested that an MG15 in the base configuration be operated at a PRF of no greater than 150-Hz. This is due to the rapid accumulation of heat within the MG15 when operated at high PRFs. Lifetime

data presented in a subsequent section will further illustrate the reason for the PRF restriction.

An MG15 in standard configuration produces an output pulse with a rise time between 4 and 6 ns. The FWHM of the output pulse is approximately 23 ns. Both the rise time and pulse width were measured into a 50-Ω load.

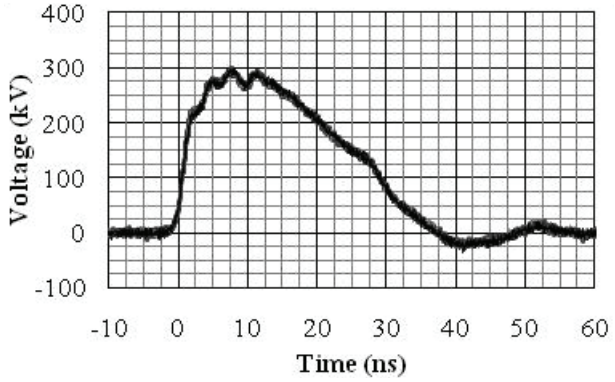

Figure 3. Superposition of 18 MG15 output waveforms measured during burst mode operation at 200-Hz PRF at maximum charge.

B. Miniaturized Configuration

APELC offers a miniaturized configuration of the MG15 when volume and weight must be kept to a minimum. This configuration sacrifices the utility of the quick-disconnect output cable, but reduces the length of the MG15 by approximately 13 cm to 81.9 cm, yielding a reduction in volume of 14%. An additional reduction in length by 5 cm is possible at the expense of further complications in servicing and manipulation of the charge and trigger cables. The output pulse characteristics and the burst mode capabilities of the MG15 are not adversely affected in the miniaturized configuration.

C. Modular Peaking Circuit

Applications such as direct RF radiation require a fast rise time (and ideally a fast fall time as well) to efficiently radiate. Certain military testing standards, such as MIL-STD 461E, also specify waveform parameters such as rise time. In an effort to meet the growing demand for a pulser capable of sub-nanosecond rise time, APELC has developed a modular peaking circuit that replaces the standard output of an MG15. The peaking circuit has been under development for 3 years and the data presented herein was obtained from the most recent hardware revision. The first generation peaking circuit was reported on in [5].

The peaking circuit requires up to 1000 psig of dry breathable air for proper operation. The peaking circuit features an aluminum housing, plastic insulation, and CuW electrodes and lengthens the MG15 by approximately 31 cm when installed. A side view of the MG15 with the peaking circuit installed is shown in Figure 1 (c).

Output waveforms from an MG15 equipped with a peaking circuit are provided in Figure 4 for three different charge voltage levels. Two standard rise time metrics are listed in Table 2 for each of the charge voltage levels. Only the output waveform from the 30-kV charge voltage level failed to yield sub-nanosecond rise time. A comparison between the output of an MG15 in standard configuration and one equipped with the peaking circuit, both operating at the 30-kV charge voltage level, is shown in Figure 5.

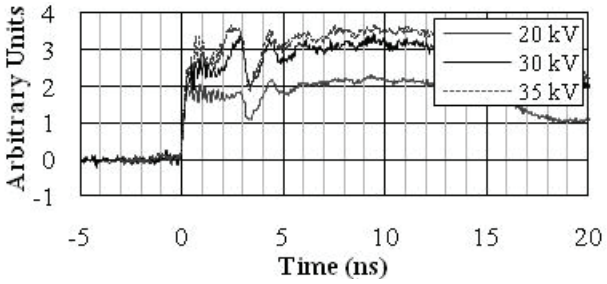

Figure 4. MG15 output waveforms realized by using the modular peaking switch. Output waveforms are provided for three different MG15 charge voltage levels.

Table 2. Summary of peaking switch performance for three different MG15 charge voltage levels.

V_{charge}	[kV]	20	30	35
t_{rise} **(10-90)**	[ns]	0.48	2.48	0.67
t_{rise} **(20-80)**	[ns]	0.22	0.85	0.59

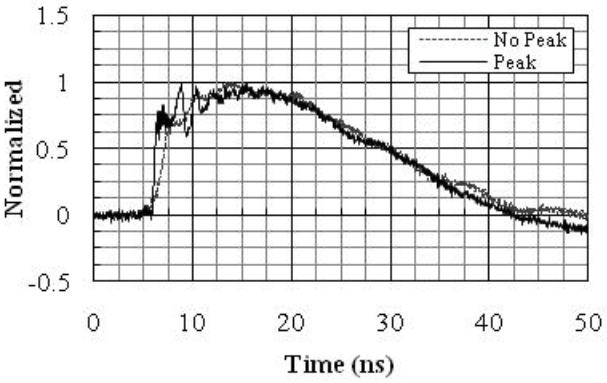

Figure 5. Direct comparison of MG15 output waveforms with (solid black) and without (dashed grey) the modular peaking circuit at a 30-kV charge voltage level.

The peaking circuit effectively reduces the rise time of the MG15 from ~4-6 ns to below 1 ns in most instances. At present, the peaking circuit is a low-repetition-rate device due to the nature of its fabrication. Efforts are underway to modify the peaking circuit for use in rep rate scenarios.

D. Support Systems

Several support systems are required for operating the MG15. A positive polarity, high voltage power supply (HVPS) with the capability to charge on demand is

required. It is preferred that the HVPS be a constant-current supply, and APELC typically recommends the Lambda 802-L for use with the MG15. The Lambda 802-L provides sufficient power to operate the MG15 at the 40-kV charge voltage level at the maximum recommended PRF.

A source of dry, breathable air is required for spark gap insulation in both the MG15 as well as the optional peaking circuit. The MG15 requires no more than 1.14 MPa of dry breathable air for operation, whereas the peaking switch can require up to 6.9 MPa of the same gas. Additionally, both the MG15 and the optional peaking circuit require unique flow rates to exchange the volume of gas during use. Due to the requirement of establishing a unique pressure and flow rate in each component, APELC offers gas flow control panels that can be sourced from a main gas supply line.

A trigger source is also required to provide a method of regulating the Marx erection event. APELC employs a trigatron trigger on the first spark gap of the MG15. A negative polarity, 18-kV pulse is applied to the center pin which ejects plasma into the first spark gap. This forces the first spark gap to breakdown which overstresses the following gap causing it to breakdown. This process progresses down the MG15 causing it to erect. APELC offers a commercially available trigger unit, the HRR-TU-18kV, which is capable of triggering the MG15 at the maximum recommended PRF.

Finally, the timing of the charge and trigger events are controlled by a model 575 BNC delay generator. Three channels of the delay generator are used to control the MG15 charge cycle, the HRR-TU-18kV charge cycle, and the HRR-TU-18kV discharge event timing.

III. MG15 PERFORMANCE

Prior to adopting the MG15 for use in a variety of platforms, potential users need critical performance-related questions answered. In an attempt to quantify acceptable dry breathable air flow rates and burst lengths, APELC performed lifetime studies on an MG15. Additionally, APELC has performed jitter measurements on the timing between when a fire command was issued by the user and when the output pulse was delivered by the MG15. Both the lifetime test and the jitter study will assist potential users in system design and in performing system lifetime estimates.

A. Lifetime Testing

In an attempt to completely characterize the performance of the MG15 while operating in burst mode, APELC fielded electrical and thermal diagnostics during a lifetime test. The lifetime test necessitated automated control of the MG15 charge and trigger events as well as automated recording of the data generated by the electrical and thermal diagnostics. A LabView controlled testbed was designed and implemented to achieve the desired level of automation. Following the development of the automated testbed, a lifetime experiment was conducted over a variety of charge voltage settings and burst mode operating points. Each unique test was referred to as a 'sequence,' and an abridged summary of test sequence data is provided in Table 3.

Table 3. Summary of lifetime test data

Seq #	V_{charge} (kV)	P_{marx} (kPa)	R_{flow} (cm^3/s)	# of pulses	PRF (Hz)
202	30	480	660	3000	200
204	20	180	660	8000	50
I017	20	280	940	1000	20
I018	20	280	1400	1000	20

Heat transfer is typically characterized by four dominant processes; conduction, convection, radiation, and mass transfer. The first thermal data presented from sequence 202 in Figure 6 depicts the temperature of the bus work nearest to the high-side electrode on the eighth and fourteenth stages of the MG15 during operation in burst mode as described by the corresponding entry in Table 3.

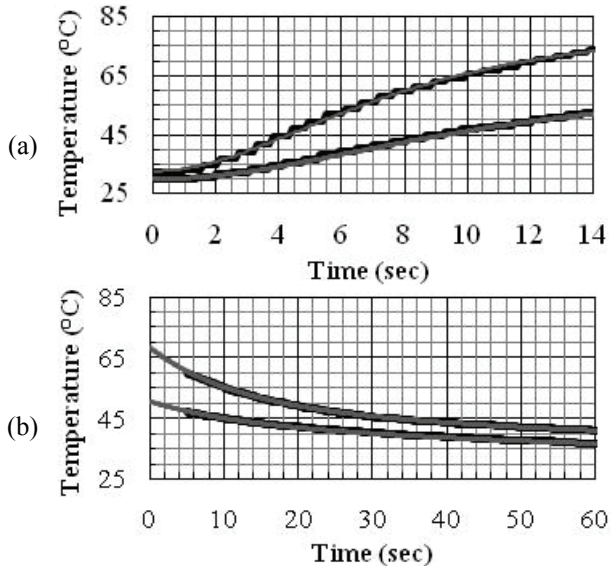

Figure 6. Thermal data acquired during sequence 202 (a) during burst-mode operation of the MG15 and (b) during the period immediately following the operation of the MG15. Sensors are located on stages 8 (cooler) and 14 (hotter). Experimental data are shown in black and curve fits are shown in grey.

Fitting the experimental data (shown in black) with an asymptotic approximations (shown in grey) during temperature accumulation, as illustrated in Figure 6 (a), indicates that only one heat transfer process dominates as listed in equations (1) and (2). It is important to note that a temperature gradient exists in the direction of the MG15 erection wave. Stated differently, the temperature of the electrodes at stage N are cooler than those at stage N+1. This is illustrated in Figure 6 (a) by the two distinct temperature curves that were acquired simultaneously.

At present, APELC believes one of two possible heat transfer processes is responsible for the accumulation of heat during burst mode operation. The first plausible explanation is that mass transfer via electron impact is the primary heat transfer mechanism responsible for temperature accumulation during operation. Electrons bridging the spark gap transfer their kinetic energy to the electrode upon which they impact creating heat. As the erection wave progresses down the stages of the MG15, electrons on the surface of the cathode of each electrode pair have a potential energy proportional to the product of the stage number and the charge voltage. During the breakdown process, the potential energy is transferred to kinetic energy of the traveling electron which then impacts the anode, heating up the electrode.

$$T_{202H}(t) = 33 + \frac{53t^2}{t^2 + 62} \tag{1}$$

$$T_{202L}(t) = 30 + \frac{35t^2}{t^2 + 115} \tag{2}$$

The second scenario that could explain the temperature gradient that exists within the MG15 is that, despite conventional wisdom, the current is non-uniform throughout the device. If the transfer rate of charge across the final gap is faster than that of the gap immediately preceding it, the current through the final gap is comparatively greater as well. Envisioning the MG15 as a Marx generator with a single current path would complicate the rationalization of this argument. If stray elements are considered, it becomes more feasible that non-uniform current could exist for brief instances throughout the device. The dominant heat transfer mechanism in this instance could be conduction due to joule heating in the arc channel.

Following the operation of the MG15, the temperature was monitored to better understand the decay rate and the heat transfer mechanisms responsible for the cooling process. The data acquired during the cooling period is presented in Figure 6 (b), and the equations modeling the exponential decay are given in equations (3) and (4). Because there is no electron flow while the MG15 is not operating, mass transfer cannot be responsible for cooling. It is believed that the buswork present inside the MG15 acts to conduct heat away from the electrode quicker than the heat can be convected away by the flow of pressurized dry breathable air through the MG15. For this reason, it is believed that the first exponential coefficient represents heat transfer via conduction; the second represents convection; and the third, radiation. Because these processes should be material dependent and because the materials used in each stage are common, the exponential constants were kept constant for both equations (3) and (4). The effectiveness of each of the heat transfer mechanisms as represented by the constants preceding each exponential term are believed to be affected by the physical conditions surrounding the stage and are adjusted accordingly. For instance, the flow of gas at stage 10 could be far more turbulent than that at stage 5.

$$T_{202H}(t) = 90 + 30e^{-(0.095t)} + 26e^{-(0.021t)} + 9e^{-(0.00125t)} \tag{3}$$

$$T_{202L}(t) = 75 + 10e^{-(0.095t)} + 19e^{-(0.021t)} + 19e^{-(0.00125t)} \tag{4}$$

An interesting contrast to the data presented in Figure 6 is that presented in Figure 7. The conditions during which the data were acquired differed vastly and is reflected in the equations derived for each of the curve fits listed in equations (5) and (6). As can be deduced from Figure 7 (a) and equation (5), slower accumulation of heat allows more heat transfer processes to participate. Conversely, as shown in Figure 7 (b) and equation (6), when a lower temperature is reached during operation, fewer heat transfer mechanisms can participate in the cooling process.

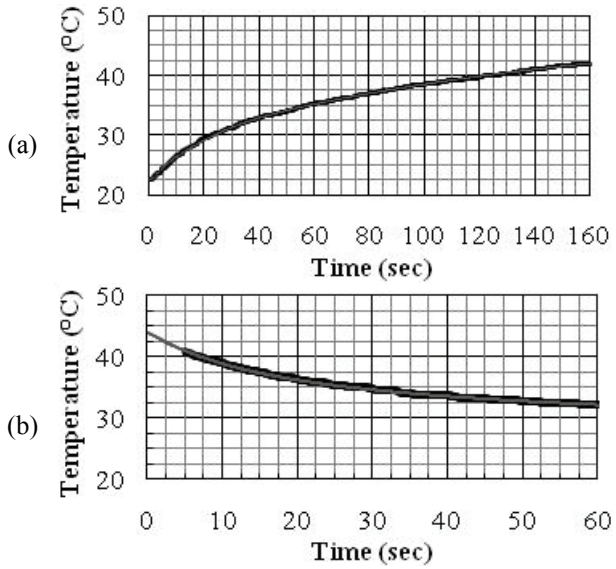

Figure 7. Thermal data acquired during sequence 204 (a) during burst-mode operation of the MG15 and (b) during the period immediately following the operation of the MG15. Experimental data are shown in black and curve fits are shown in grey.

$$T_{204}(t) = 72.5 + \frac{6.3t^2}{t^2 + 28} + \frac{15.3t^2}{t^2 + 700} + \frac{24.75t^2}{t^2 + 20000} \tag{5}$$

$$T_{204}(t) = 85.55 + 10.35e^{-(0.095t)} \tag{6}$$

Sequences I017 and I018 were performed at different flow rates with all other parameters held constant. Results of both test sequences are presented in Figure 8. It is evident that, while a higher flow rate keeps the MG15 from reaching a higher internal temperature, the reduction in accumulated temperature achieved by raising the flow rate is nearly negligible in the example shown in Figure

8. Therefore, the potential volume and weight reduction achieved by using a lower flow rate likely outweighs the benefit of a higher flow rate in a deployment scenario. Additionally, the data presented in Figure 8 further validates the belief that conduction is the dominant heat transfer mechanism during the cooling process as the temperature is only marginally affected by a 33% increase in flow rate.

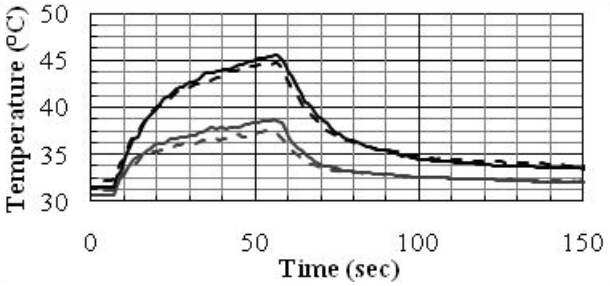

Figure 8. Thermal data acquired during sequences I017 (solid lines) and I018 (dashed lines). Sensors are located on stages 8 (grey) and 14 (black). Curve fitting was not performed for this data.

Given the data presented in Figure 6, Figure 7 and Figure 8 (and data similar to it), estimates can be made on acceptable burst durations and required cooling time. APELC is compiling the data acquired during the lifetime study to attempt to better define acceptable burst mode operational parameters.

B. System Jitter

The need occasionally arises for low-jitter operation of the MG15. Two examples of this are when multiple MG15s are used simultaneously, or when synchronizing the MG15 with other equipment. The jitter results presented in Figure 9 illustrate a reference point from the model 575 BNC delay generator (black trace) and the MG15 output waveform (grey trace). A total of 21 event pairs are plotted in Figure 9. The results of the study are summarized in Table 4. The results of the first test, Test 1, were first presented in [2] and validated again in subsequent testing, Test 2.

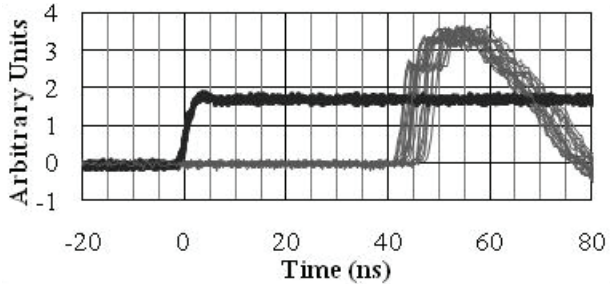

Figure 9. Data acquired during the first jitter study test. The black waveforms are the fire command reference signals from the model 575 BNC delay generator and the grey waveforms are the output waveforms from the MG15. A total of 21 waveform pairs are plotted.

Table 4. Summary of jitter study test results.

Test #	Jitter [ns]
1	1.84
2	1.21

IV. CONCLUSIONS

APELC has designed a robust and versatile Marx generator (the MG15-3C-940PF) that has fulfilled the needs of many customers for a wide variety of applications. The MG15's price point and reliability are a welcome benefit to its many users. The ease with which the MG15 can be customized to meet the varying needs of its users is also advantageous. The MG15 has demonstrated reliable operation at extreme burst rates for long durations and has demonstrated the capability to operate with sub nanosecond rise time. The system that accompanies the MG15 has demonstrated a system jitter of less than 2 ns.

APELC is continually working to improve the MG15. Presently an internal lifetime study is continuing with an MG15 fabricated with more robust internal insulation. The goal of the study is not only to identify new thermal limitations, but also to identify the minimum acceptable flow rates for deployment scenarios.

V. REFERENCES

[1] C. Nunnally, M. Lara, J. R. Mayes, T. R. Smith, "Low Cost 400-ps Rise-Time Circuit-Board Marx Generator," these proceedings.

[2] T. A. Holt, et al., "Marx Generators for High-Power RF and Microwave Applications," in proceedings of the IEEE Power Modulator and High Voltage Conference, Atlanta, GA, 2010.

[3] J. R. Mayes, C. W. Hatfield, and J. D. Dowden, "Development of a Dual-Polarity Marx Generator Designed for Pulse Charging a Dipole Antenna," in proceedings of the IEEE Power Modulator and High Voltage Conference, Atlanta, GA, 2010.

[4] T. A. Holt, et al., "Modular, High-Power, Wideband Transmitters for Electromagnetic Environmental Effects (E3) Testing," these proceedings.

[5] T. A. Holt, et al., "Compact Marx Generators Modified for Fast Risetime," in proceedings of the 17th IEEE International Pulsed Power Conference, Washington, DC, 2009, pp. 1197-1200.